Stochastic perturbations and dimension reduction for modelling uncertainty of atmospheric dispersion simulations

Sylvain Girard[a,*], Patrick Armand[b], Christophe Duchenne[b], Thierry Yalamas[c]

[a] *18 boulevard de Reuilly, Phimeca, France*
[b] *CEA, DAM, DIF, F-91297 Arpajon, France*
[c] *Centre d'affaires du Zénith, 34 rue de Sarliève, 63800, Cournon d'Auvergne, France*

Abstract

Decision of emergency response to releases of hazardous material in the atmosphere increasingly rely on numerical simulations. This paper presents two contributions for accounting for the uncertainty inherent to those simulations. We first focused on one way of modelling these uncertainties, namely by applying stochastic perturbations to the inputs of the numerical dispersion model. We devised a generic mathematical formulation for time dependent perturbation of both amplitude and dynamics of the inputs. It allows a more thorough exploration of possible outcomes than simpler perturbations found in the literature. We then improved on the current state of the art on dimension reduction of atmospheric data. Indeed, most statistical methods cannot cope with high dimensional data such as the maps simulated with atmospheric dispersion models. Principal component analysis, the most widely used method for dimension reduction, relies on a linearity hypothesis that is not verified by these sets of maps. We conducted a very encouraging experiment with auto-associative models, a non-linear extension of this method.

Keywords: atmospheric dispersion, uncertainty propagation, wind field, time warp, perturbation

*Corresponding author

Email addresses: girard@phimeca.com (Sylvain Girard), patrick.armand@cea.fr (Patrick Armand), christophe.duchenne@cea.fr (Christophe Duchenne), yalamas@phimeca.com (Thierry Yalamas)

1. Introduction

Decision of emergency response to releases of hazardous material in the atmosphere increasingly rely on predictions from numerical models. Such simulations of atmospheric dispersion are highly uncertain due to the complexity of the physical phenomena, and because their inputs, in particular meteorological or source term related, are highly uncertain. We propose two methodological improvements to the current practices aimed at accounting for these uncertainties.

In section 2, we state the importance of setting the decision problem in a probabilistic framework, and introduce a realistic case study later used to illustrate our two contributions.

In section 3 we expound on one way of modelling these uncertainties, namely by applying stochastic perturbations to the inputs of the numerical dispersion model. We devised a generic mathematical formulation for time dependent perturbation of both amplitude and dynamics of the inputs. It allows a more thorough exploration of possible outcomes than simpler perturbations found in the literature.

The output of dispersion models are spatial maps. Analysing a set of maps, whether qualitatively by visual inspection, or quantitatively with statistical methods, is much harder than dealing with numerical values. In section 4 we discuss the issue of obtaining a concise representation of maps by a few scalars. Principal component analysis is the most widely used method for dimension reduction. It relies however on a linearity hypothesis that is seldom verified by sets of maps produced by dispersion models. We conducted an encouraging experiment with auto-associative models, a non-linear extension of this method.

Both sections 3 and 4 begin with a detailed survey of the literature on the topic at hand.

2. Problem statement

We consider the following idealised decision problem. Hazardous material is released in the atmosphere during a given period of time. Mitigation actions, for instance population sheltering or evacuation, must be performed in areas where a given concentration threshold is exceeded. Theses concentrations are predicted with a physical model simulating transport and dispersion in the atmosphere, and deposition by rain.

This decision making scenario is inspired by a real industrial incident that happened on January 2013 at the Lubrizol chemical plant located in Rouen, France. Operation mistakes and minor system failures in the plant resulted in extended release of hydrogen sulphur and mercaptan, which are both foul-smelling. The first report of olfaction in the neighbourhood of the site occurred at 8:00 am (local time) on Monday 21 January 2013. The first major emission peak occurred 12 hours later (2013-01-21 20:00). The major part of the material inventory (99%) was emitted during 23 hours, between 2013-01-21 13:30 and 2013-01-22 12:30 [19]. The wind blew the plume as far as Paris during Monday night and towards London on Tuesday. Thousands of people have complained of nausea and headaches. For practical reasons, we focused here on a restricted area of about 35 kilometres horizontal print. Our approach could equally be applied at different space scales.

2.1. Physical model

The dispersion simulations were carried out with Parallel-Micro-SWIFT-SPRAY (PMSS). Originally, Micro-SWIFT-SPRAY (MSS) [33] was developed in order to provide a simplified but rigorous computational fluid dynamics solution of the flow and dispersion over rugged terrains and built-up environments in a limited amount of time. MSS encompasses the local scale high resolution versions of the SWIFT and SPRAY models.

SWIFT is a 3D terrain-following mass-consistent diagnostic model taking account of the buildings and providing the 3D fields of wind, turbulence, and temperature. SWIFT interpolates between meteorological measurements (ground stations and vertical profiles), numerical data issued by meso-scale simulations (as in this paper) and, possibly, analytical relations of the flow influenced by the buildings (displacement zone, wake zone, skimming zone, etc.).

SPRAY is a 3D Lagrangian Particle Dispersion Model able to account for the presence of buildings. Both SWIFT and SPRAY can deal with complex terrains and evolving meteorological conditions and with specific features of the release (heavy gas, light gas, etc.). More recently, SWIFT and SPRAY have been efficiently parallelized in time, space, and numerical particles leading to the PMSS modelling system [28]. PMSS has been thoroughly validated against several wind tunnel and in-field experimental campaigns in the framework of notably the European COST Action [34] and the UDINEE project [27]. The performances of PMSS give full satisfaction as the modelling system is compliant with the validation criteria for 3D dispersion models adapted to built-up areas, proposed by Hanna and Chang [16] and used internationally,

2.2. Deterministic decision map

The source is located in the middle of the simulation domain, parallelepiped whose horizontal print is a square with edge of 35 km. The simulation duration was set 35 hours in order to ensure that all material has either been deposited or exited the simulation domain at the end of simulation. In a deterministic framework, a single simulation is run using the most credible values for the meteorological and source term model inputs. From now on, we call this set of values the (input) conjecture, and likewise we refer to the concentrations simulated using them as conjectured concentrations. We focus here on three uncertain inputs known to have a substantial impact on simulation output [3, 14, 2, 15]:

- the rate of emission of material is a time series, called source term,
- the rain intensity is a scalar spatio-temporal field,
- and wind velocity (speed and direction) is a vector spatio-temporal field.

The conjectured source term, displayed on figure 1, was adapted from data established by Ismert and Durif [20].

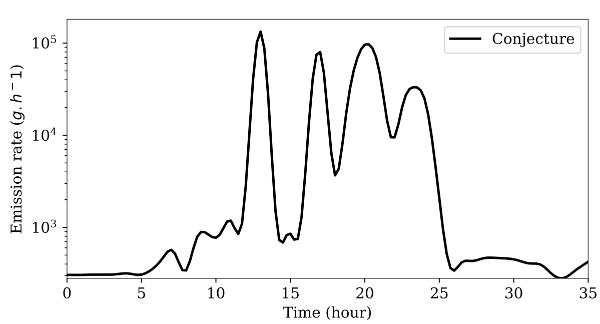

Figure 1: Conjectured source term. The time abscissa starts on 21 January 2013, 7:00.

The conjectured rain and wind fields were obtained from the community reconstruction weather and forecast meso-scale modelling system WRF [31]. The WRF simulation domain has a horizontal resolution of 1 km. For the wind, we used a set of 514 vertical profiles of the horizontal components, and we kept the 21 vertical layers below 3 km above ground level (AGL), plus surface data at 10 m AGL. Their locations are displayed in figure 2. WRF simulations are sampled every 15 minutes, and we used the 141 time steps from 21/01/2013 07:00 to 22/01/2013 18:00.

We want to predict, at each location, whether an arbitrary concentration threshold of $2\mu\, g \cdot cm^{-3}$ is exceeded during the considered 35 hour time frame. In real application, this decision criterion could correspond for instance to olfaction threshold or important health damage. The area where the concentration threshold is exceeded during the conjecture simulation is coloured in dark red in figure 2. Note that in this example, we do not consider the actual olfactory limit of the mercaptan which is lower than the chosen threshold and would lead to a decision map spanning quite all over the simulation domain, thus making less interesting the visual presentation of the uncertainties influence on the decision map.

2.3. Probabilistic decision map

We tackle the decision problem stated above from the viewpoint of uncertainty propagation. We need the probability distribution of maximum concentrations, but cannot model it directly. Instead, we model the uncertainty of inputs of the physical model by stochastic perturbations. The atmospheric dispersion model is a deterministic function. Here, its inputs are the source term, and the rain and wind fields. Its output is the maximum concentration over time at each location. Figure 3 represents the chain of functions linking the random variables of the problem. The random vector of perturbed inputs is denoted by Y, and the simulated maximum concentration over time by $Z(s)$, a function of the location s. The upstream part of the chain will be described in section 3.

In a probabilistic framework, taking a decision implies to admit a risk of committing a specified error. We choose here the risk of deciding not to perform a mitigation action while the concentration threshold is actually exceeded. The corresponding probabilistic decision rule is to decide action where the estimated probability of exceedance is above a small arbitrarily specified value, for instance 5%. The other possible error, not considered here, would be to decide unnecessary actions.

Exceedance maps are obtained from maximum concentration maps by setting each cell to 1 if the chosen threshold is exceeded and 0 otherwise. Averaging a set of exceedance maps yields a Monte Carlo estimator of the

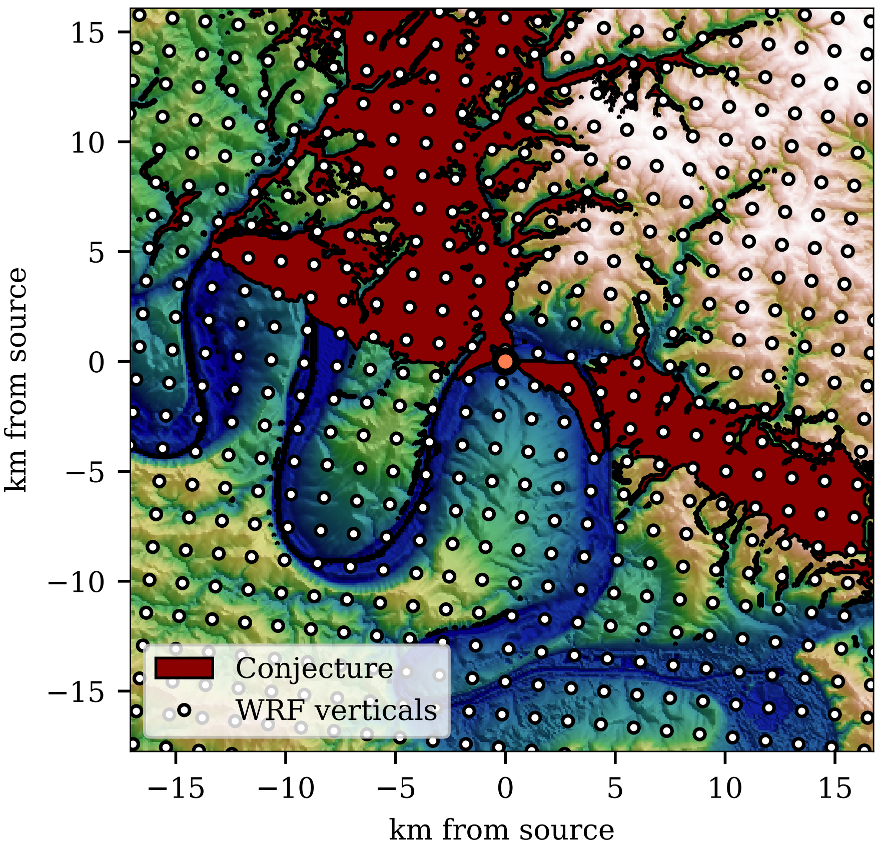

Figure 2: Area where the concentration threshold is exceeded during the conjecture simulation (dark red). The source location is indicated by an orange dot. White dots indicate the locations of the WRF verticals used as meteorological conjecture.

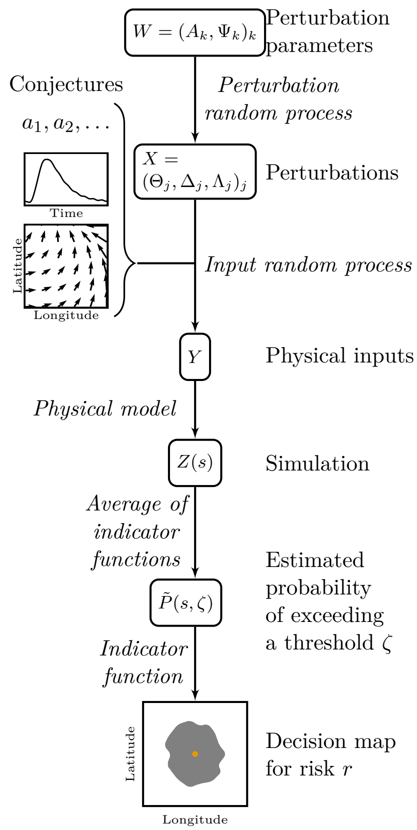

Figure 3: Function chain of the uncertainty propagation. Capital framed letters designate random vectors. Arrows annotated in italic designate functions.

probability of exceedance. Figure 4 displays probability of exceedance thus estimated from a sample of 100 simulations with inputs perturbed as described in section 3. This relatively small sample size is representative of crisis context when decision must be taken rapidly while each simulation requires up one hour of computation as in our case study. Assessing the convergence of the estimator of small probability with small samples is not trivial [1], but we expect errors due to partial convergence. Therefore, a conservative stance is to draw a decision boundary enclosing the level set corresponding to the chosen probability threshold (for instance the black line separating green and yellow in figure 4, for a 5% threshold).

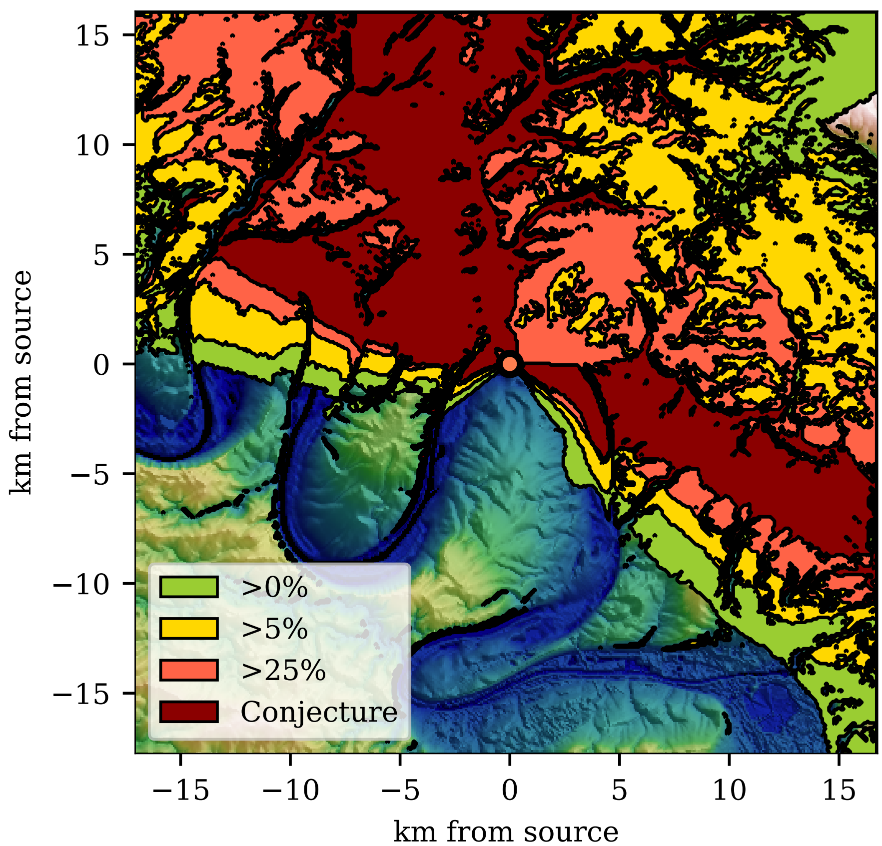

Figure 4: Orange, yellow and green areas correspond to three intervals for the probability of exceedance estimated from 100 simulations.

3. Amplitude and dynamics perturbation scheme

We will now describe specifically the perturbation model. In section 3.1, we review the rationale behind modelling uncertainty by stochastic perturbations and the state of the art. In section 3.2, we present our generic mathematical formulation for amplitude and dynamics perturbations. Finally, in section 3.3 we detail how it was implemented for the case study.

3.1. Uncertainty modelling by stochastic perturbations

The input conjecture comprises any model input that is issued from partial or imprecise observations, or from other physical model simulations, and possibly also model parameters that implicitly account for the unavoidable discrepancy between the real complex system under study and its idealised mathematical representation.

One possible approach to modelling those uncertainties is to apply stochastic perturbations to the input conjecture. The meteorological conjecture is usually obtained from simulations with meteorological models. Several authors suggested to apply uncertainty propagation to those models, or to use sets of different models to produce build ensembles of input meteorological conditions [35, 10]. However, as [7] points out, it is rather unlikely that such an ensemble of conjectures might be available in a crisis context. Indeed, considerable efforts must be spent to calibrate such ensembles [11, 36], and the calibration process requires reference data that are not available when dealing with accidental releases. It can be expected that using ensembles designed for meteorological forecast as a substitute for specifically calibrated ones would result in underestimation of uncertainty. However ensemble approach and conjecture perturbations are not mutually exclusive: applying additional perturbations to the ensemble members could possibly retrieve the missing variability [23]. We focus here on the case when a single conjecture is available.

Random perturbations of inputs commonly found in the literature [7, 4, 17, 12, 14, 15] are time independent random variables. They often follow a Gaussian distribution for additive perturbation, and log-normal for multiplicative perturbation. The dynamics of the conjecture is rarely perturbed, except sometimes by global time delays [14, 15].

3.2. General mathematical formulation

The conjecture is, in general, a set of data of diverse dimensions: scalars, time series, and spatio-temporal fields. They are grouped by a brace on figure 3. The random perturbations, collectively denoted by X on figure 3, are functions of the set of random perturbation parameters W.

More precisely, let $Y(s,t)$ be the spatio-temporal random vector obtained by perturbation of a conjecture $c(s,t)$. We adopted the following generic perturbation:

$$Y(s,t) = \Gamma(s, \Theta(t))\ c(s, \Theta(t)) + \Delta(s, \Theta(t)). \tag{1}$$

The random vector Γ (respectively Δ) is a multiplicative (respectively additive) perturbation of the amplitude of the conjecture, that we will call the "gain" (respectively "offset") perturbation. The random function Θ is the perturbation of the dynamics of the conjecture, called "time warp" perturbation.

3.2.1. Spatio-temporal structure of the perturbation

The spatio-temporal structure of each component of the perturbation must be postulated. We chose to impose smooth oscillating temporal variations, and have the perturbation depend on the location only through the conjecture. More precisely, we used sums of cosines

$$\sum_{k=1}^{K} A_k\ cos(2\pi\omega_k t + \Psi_k). \tag{2}$$

with random phases $\Psi_1, \ldots, \Psi_k$, and random amplitudes $A_k, \ldots, A_K$. The time structure of the random process is controlled by the choice of the K periods $\omega_k, \ldots, \omega_K$. The value of K is itself a parameter to be chosen by the modeller.

The phases are independent and uniformly distributed on $[0, 2\pi]$. The distributions of the amplitudes are arbitrary.

The gain and offset random processes are directly given by equation (2). The additional derivation of the time warp process is detailed in the next section.

3.2.2. Time warp

Let $\phi : \mathbb{R}^+ \times \mathbb{R}^+ \mapsto \mathbb{R}^+$ be a function that expands or contracts a time interval δt by a factor $\lambda(t)$ that varies in time:

$$\phi : t, \delta t \mapsto \phi(t, \delta t) = \lambda(t)\, \delta t. \tag{3}$$

Let $\{0 = t_0 < t_1 < \cdots < t_q = T\}$ be a sequence of instants interspersing a time frame of duration T. Denote by $\phi_0, \ldots, \phi_{q-1}$ the warped time intervals:

$$\phi_n = \phi(t_n, t_{n+1} - t_n). \tag{4}$$

The associated *time warp* function $\theta : \mathbb{R}^+ \mapsto \mathbb{R}^+$ preserves the time origin and warps subsequent instants:

$$\theta(t_0) = t_0 = 0, \tag{5}$$

and $\forall n : 1 \leq n \leq q-1$,

$$\theta(t_n) = \frac{T}{\sum_{i=0}^{q-1} \phi_i} \sum_{i=0}^{n} \phi_i. \tag{6}$$

It follows from the above definition that a time warp function also preserves the total duration: $\theta(t_q) = t_q = T$.

A time warp random process Θ is fully characterised by specifying a random process Λ for generating warping factors $\lambda(t)$. We used smoothly oscillating functions as defined by equation (2). In practice, a warped time series (namely a realisation $y(s,t)$ of the random function $Y(s,t)$ in equation (1)) is obtained by

1. Applying the gain and offset perturbations to the conjecture.
2. Sampling warping factors $\lambda(t)$ from Λ.
3. Computing the corresponding warped instants $\theta(t_0), \theta(t_1), \ldots, \theta(t_q)$.
4. Interpolating the time series resulting from step 1 at the warped instants.

3.3. Perturbations for the case study

We perturbed four input conjectures by processes based on equation (1):

- source term (gain and time warp),
- rain intensity (gain and time warp),
- wind speed (offset and time warp),
- and wind direction (offset and time warp).

Component	Criterion
All time warps	95% of the values lag behind (or anticipate) the corresponding conjectured value by less than 2 hours.
Source term gain	95% of the gain factors (as time varies, and from one realisation to another) are between 0.5 and 2, with a median equal to 1.
Rain intensity gain	95% of gain factors (as time varies, and from one realisation to another) are between 0.5 and 2, with a median equal to 1.
Wind speed and direction offsets	95% of offsets lie within an interval whose length depends on the spatial average of wind speed in each vertical layer at each time step.

Table 1: Calibration criteria for the amplitude distributions.

This amounts to a total of 8 random functions (2 gains, 2 offsets and 4 time warp). All these components of the perturbation processes are statistically independent. They have all the same temporal structure, with $K = 3$ periods. Each component thus involves 6 random variables: 3 phases and 3 amplitudes (see equation (2)). The total number of random variables is $8 \times 6 = 48$.

We choose the following values for the periods: $\omega_0 = 0$, $\omega_1 = T/4$ and $\omega_3 = T$ (the simulation time frame T is equal to 35 h). They induce contributions to the perturbation that are respectively, constant in time, with 4 cycles within the time frame, and with a single cycle.

We used independent Gaussian random variables with zero mean for all amplitudes (denoted A_k above). We applied an exponential transformation to the gain perturbations. The resulting distributions of multiplicative factors are thus roughly log-normal with median equal to 1. The standard deviations were determined following the criteria listed in table 1 established by expert judgement. Refer to supplementary material for illustrations.

4. Dimension reduction of a set of maps

Precise estimation of small probabilities of exceedance require larger sample size than what can usually be achieved in a crisis context, due to the substantial CPU cost of detailed atmospheric dispersion models. Furthermore, input uncertainty models rely on many postulates, for instance the distribution of perturbation parameters. The robustness of the decision criterion can be tested by repeating the uncertainty propagation with different sets of perturbation parameters, which would require even greater sample size. Sample size can be a limiting factor even in less time constrained contexts like sensitivity analysis [14, 15] and source term estimation by inverse methods (Liu, 2017).

Model emulation is an alternative to direct estimation by Monte Carlo sampling [3, 2, 15, 26, 24, 25]. The simulation sample is used to build a mathematical approximation of the physical model whose computational cost is negligible. Emulation techniques, such as Gaussian process regression [30] apply to models with a scalar output, but the output of the physical model considered here is a spatial map. In practice it is represented by a large number of values sampled on the nodes of a grid, in the same manner that a raster image is a set of pixels. Because these node variables are intricately dependent on one another, we can attempt parametrising the maps with a lesser number of variables by a process similar to those used for image compression.

Principal component analysis (PCA) is a method for dimension reduction used extensively in data analysis for more than a century [29, 21]. It can be considered as the state of the art for dimension reduction in the specific field of dispersion simulation [6, 32, 26, 24, 25]. However, it relies on a linearity hypothesis that is not verified by the set of maps typically produced by atmospheric dispersion models. We expound on this issue in section 4.1.

Auto-associative models (AAM) are a non-linear extension of PCA that benefits from an explicit and attractive mathematical foundation [13]. It is presented in section 4.2, and its performance is compared to that of PCA in section 4.3.

4.1. Limitations of principal component analysis

The output of the dispersion model is a spatial map (denoted by $Z(s)$ in figure 3) discretised on a grid with p nodes. As such, it can be seen as a p dimensional vector, and the set of output maps $\mathcal{Z}$ is a subset of $\mathbb{R}^p$. The principle of dimension reduction is to build an approximate low dimensional system of coordinates for $\mathcal{Z}$ based on a sample of elements $z_1, \ldots, z_N$. We will assume without loss of generality that the sample point cloud is centred on the origin. Otherwise, the procedures described in the following must simply be preceded by a translation of vector $\pm\frac{1}{N}\sum_{i=1}^{N} z_i$

The algorithm of PCA solves a sequence of optimisation problems:

For $k = 1, \ldots, p$, find the unit vector a_k orthogonal to any a_i with $i < k$ that maximises $\sum_{i=1}^{n}(a'_k\, z_i)^2$ (where a'_k denotes the transpose of a_k).

For any dimension d, the principal directions $a_1, \ldots, a_d$ form an orthonormal basis of a linear space $\mathcal{L}_d$ approximating $\mathcal{Z}$. The low dimensional coordinates are simply the coordinates in this basis. We call *residual* the difference $z - \sum_{i=1}^{d}(a'_i\, z)a_i$ between an element of $\mathcal{Z}$ and its approximation.

It can be shown that $\mathcal{L}_d$ is such that

- the sum of squares of the sample residuals is minimised,
- the sum of squares of the Euclidean distances between sample points is best preserved by projection.

A major advantage of PCA is that those equivalent optimisation problems have a closed form solution: the (a_i) are the eigen vectors of $\frac{1}{N}\mathrm{Z}'\mathrm{Z}$, where Z is the $N \times p$ matrix whose rows are the (z_i).

PCA is efficient, in the sense that it yields good low dimensional approximations, when the relations between the p original variables are linear. Unfortunately, this is seldom verified when the p original variables are sampled on a time series or a spatial map.

Consider for instance a set of time series consisting of a single identical bell shaped pulse occurring at varying instants. Discretising it at p evenly spaced abscissas yields a p dimensional point cloud as before. This simple example devised by Fukunaga and Olsen [9] is actually representative of many situation common in atmospheric dispersion: time evolution of a concentration when a plume passes over a recording station, or comparison of circular cross sections of plumes with differing orientations. The minimum number of parameters needed to reversibly encode a data set without loss of information is often referred to as its “intrinsic dimension” [18]. Here, it is equal to 1. Indeed, a single scalar, say the abscissa of the top of the bell, is sufficient to fully parametrize the set of curves. However, the number of principal directions required to achieve a good approximation is close to p. In a previous communication [8], we applied PCA to sets of dispersion simulations resulting from low dimensional perturbations. While the first two or three principal components carried much more information than the subsequent ones, at least a dozen of them were required to properly encode the original dataset. This lack of efficiency even with simple perturbations shows that PCA is not well suited for analysing the output of complex perturbation schemes.

4.2. Non linear dimension reduction with auto-associative models

The algorithm for building an AAM starts with the $N \times p$ sample data matrix $\mathrm{Z}_1 = \mathrm{Z}$ whose rows are the (z_i), and repeats the following steps for $k = 1, \ldots, p$:

1. Find a direction a_k minimising a loss function.
2. Compute the vector of projection coordinates $c_k = \mathrm{Z}_k$.
3. Estimate the recovery function r_k, namely an approximation of the function linking the components of c_k to the rows of Z_k.
4. Set $\mathrm{Z}_{k+1} = \mathrm{Z}_k - \tilde{\mathrm{Z}}_k$, where $\tilde{\mathrm{Z}}_k$ is the $N \times p$ sample data matrix whose rows are the images of the projection coordinates by r_k.

Following the recommendations of Girard and Iovleff [13], we used a loss function that best preserves nearest neighbours, and built the recovery (r_k) with cubic splines. Note that PCA is a linear special case of AAM with the loss function given in the previous section, and the linear maps $r_k : \alpha \mapsto \alpha\, a_k$ for recoveries.

It was shown theoretically that AAM surpasses neural networks with simple architectures such as auto-associative perceptron with one hidden layer [13]. More sophisticated networks seem capable of good performances [22], but they require large training samples. AAM is less inductive, but its added rigidity makes it able to cope with small training samples. In that respect, our approach is closer to that of Bowman and Woods [5].

4.3. Compared performances of PCA and AAM

An important feature that one expects from a good dimension reduction technique is the fidelity of the projected data to the original. The quadratic mean of the residuals (the difference between projected and original data) is a common measure of the missing information in the projection. As a matter of fact, principal components are the solution of the minimisation of this very quantity. It is also common to normalise this measure by the variance of the original data. Indeed, when the data are realisations of random variables, the quadratic mean of the residuals is an estimate of the associated variance. This allows computing the amount of the overall variance that is explained by each projection direction. Following Girard and Iovleff [13], we call “information ratio” the sum of the variances explained by a set of directions.

Figure 5 compares the information ratios of the AAM and PCA projections of increasing dimension. It shows that the first few AAM directions are much more informative than that of PCA. Indeed, AMM is able to account for almost 80% of the data set variance with two parameters only, while PCA needs six directions to catch up with this value.

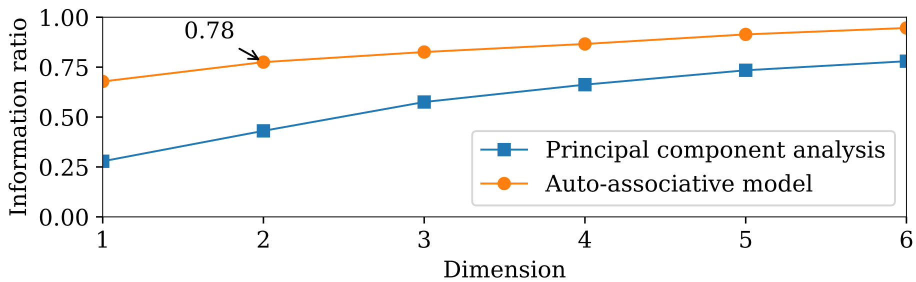

Figure 5: Information ratio of the AAM and PCA projections of increasing dimension.

In the following paragraphs, we compare in more details the AAM and PCA 2 dimensional projections. We chose to leave aside subsequent directions for three reasons:

- 2D projections can be plotted and are therefore better suited for our illustrative purpose.
- The limited size of the training sample, 100 simulations, induces a significant risk of overfitting. Cross-validation showed indeed that the third AAM direction is unreliable for extrapolation.
- Very low dimensional projection (3D and below) are the most versatile. Many methods stop working in dimension 4 and above.

Each row of figure 6 shows a group of three simulated maps whose projections are close to one another in the 2D AAM coordinate system. They are labelled by coloured letters that locate them the scatter plot of the 2D AAM coordinate system in figure 7. The simulated maps within a group are similar, while maps from different groups are dissimilar. Each groups can be characterised by the main features of the exceedance area (contoured in pale red), namely an extension towards the south-east direction, and the direction and width of the northern fan shaped area. These observations suggest that

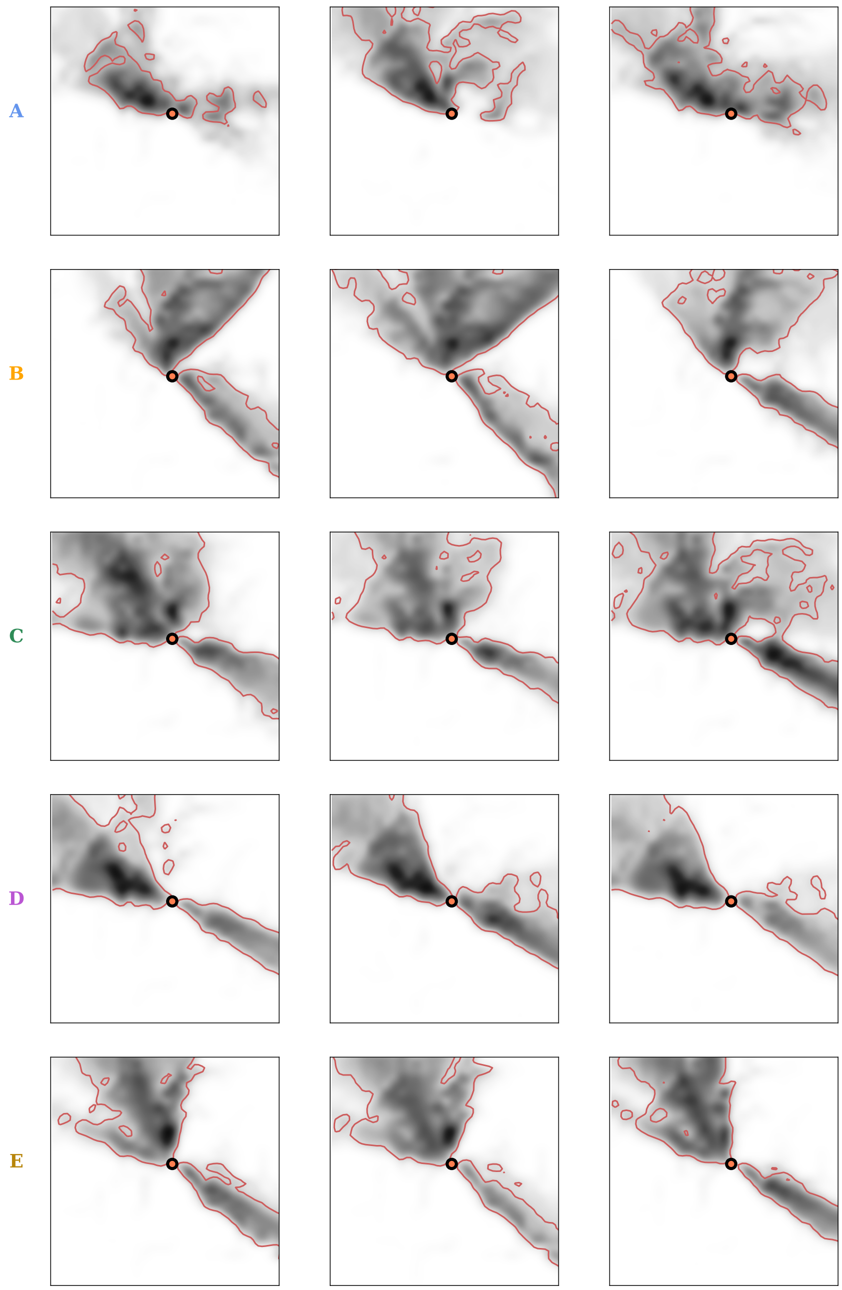

Figure 6: Five groups (in rows) of three (in column) simulated maps of maximum concentration. Grey shades denote maximum concentration (log transformed for legibility). The areas of threshold exceedance are contoured in pale red. Groups locations in the 2D AAM coordinate system are marked by large coloured circles in figure 7.

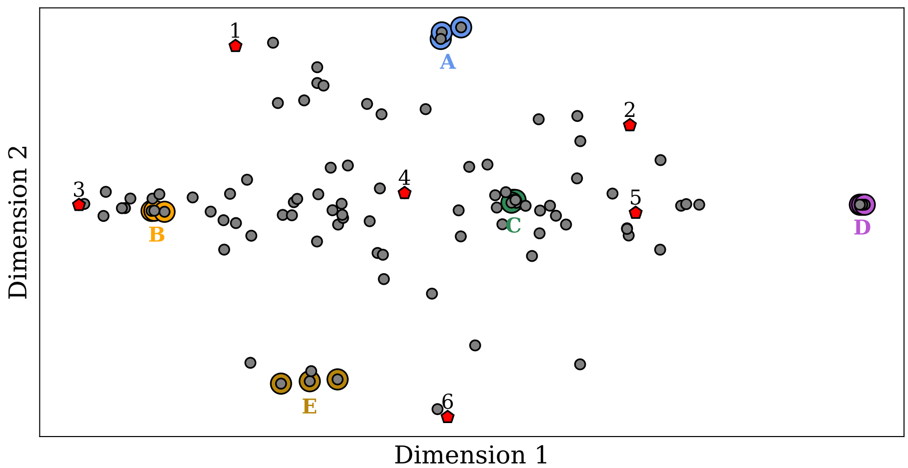

Figure 7: Scatter plot of the 100 simulations projected in the 2D AAM coordinate system. Each grey dot or red pentagon represents one simulation. Coloured circle and red pentagons highlight sets of simulations referenced in the text.

2D AAM coordinate system is able to capture the overall structure of the data set.

The left and right plots of figure 8 compare the errors induced by 2D projection with PCA and AAM respectively. Each row corresponds to one simulation whose location in the 2D AAM coordinate system is marked in figure 7 by the red pentagon with corresponding number. Green tint indicates area where exceedance is correctly predicted after projection. Orange (respectively purple) tint indicates area of false positives (respectively negatives). A false positive (respectively negative) understands here as exceedance (respectively non exceedance) at a given location in the projected map when the threshold is not exceeded (respectively exceeded) in the original map. These examples show that AAM almost always outperform PCA: the orange and purple areas in the right column are smaller than in the right. AAM even achieve perfect reconstructions in some regions of the 2D coordinate system, for instance the row 1, 3 and 6 of figure 8. These observations also apply to the other areas of the 2D coordinate system not shown here.

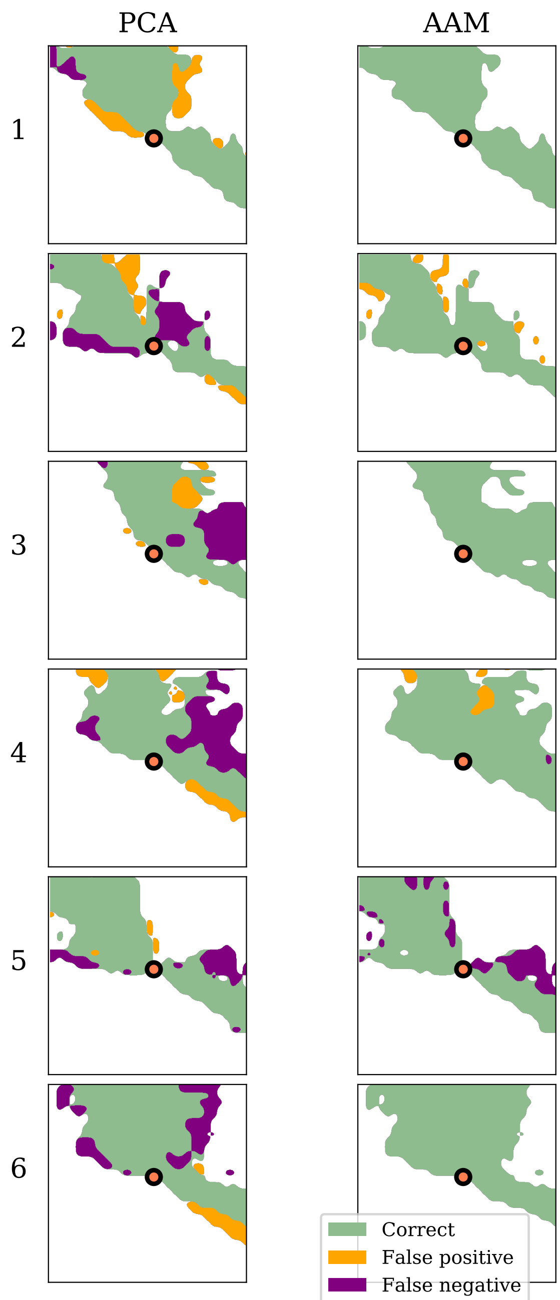

Figure 8: Comparison of errors induced by projection with PCA (left column) and AAM (right column). Each row correspond to a given original map, whose locations in the 2D AAM coordinate system are marked by numbered red pentagon in figure 7.

5. Conclusion

We proposed a generic mathematical framework aimed at modelling uncertainties in 3D atmospheric dispersion simulations. It relies on stochastic perturbations of both the amplitude and dynamics of the physical model inputs time series. These perturbations have a tuneable temporal structure, allowing for more refined uncertainty modelling than the constant perturbation of amplitude only that prevails in the literature.

To exemplify the practical use of the method, we considered a complex accidental situation on a rough and built-up terrain characterized by uncertain release and meteorological conditions (wind direction, wind speed and precipitations). This realistic case study showed that the probabilistic decision map obtained by uncertainty propagation can significantly impact decision.

The main open issue with uncertainty propagation is the limited sample size than can be achieved in the short time spans characteristic of crisis contexts. In such situations, reliable exceedance probability estimates require more advanced methods, such as model emulation. This raises another difficulty, namely that those methods apply to scalar output models, not model whose output is a spatial map. We argued that PCA, despite its ubiquitous usage, is ill fitted for dimension reduction of such data sets, but showed that AAM can overcome the shortcomings of PCA. The next step will be to leverage AAM dimension reduction to build an emulator. A possible approach is to build one emulator for each AAM coordinate, for instance using Gaussian process regression.

Contrary to situations where data is available, the structure of uncertainty models used in crisis contexts are mostly postulated. The motivation for adding a temporal structure to perturbations is to explore more exhaustively the possible outcomes of an accident. A topic for future experimentation would be to assess the relative influence of the parameters controlling that structure, and compare probabilistic decisions obtained with uncertainty models of increasing complexity. The choice of appropriate metrics for comparing decision boundaries is itself an interesting matter of investigation. AAM could provide additional comparison criteria based on topological properties of the set of output maps.

References

[1] Agresti, A., Coull, B. A., may 1998. Approximate is better than "exact" for interval estimation of binomial proportions. The American Statisti-

cian 52 (2), 119–126.
URL https://doi.org/10.1080/00031305.1998.10480550

[2] Aguirre Martinez, F., Caniou, Y., Duchenne, C., Armand, P., Yalamas, T., 2016. Probabilistic assessment of danger zones associated with a hypothetical accident in a major French port using a surrogate model of CFD simulations. In: 17th International Conference on Harmonisation within Atmospheric Dispersion Modelling for Regulatory Purposes, HARMO17. Budapest, Hungary.

[3] Armand, P., Brocheton, F., Poulet, D., Vendel, F., Dubourg, V., Yalamas, T., 2014. Probabilistic safety analysis for urgent situations following the accidental release of a pollutant in the atmosphere. Atmospheric Environment 96 (0), 1–10.
URL http://www.sciencedirect.com/science/article/pii/S1352231014005433

[4] Beekmann, M., 2003. Monte carlo uncertainty analysis of a regional-scale transport chemistry model constrained by measurements from the atmospheric pollution over the paris area (ESQUIF) campaign. Journal of Geophysical Research 108 (D17).
URL https://doi.org/10.1029/2003jd003391

[5] Bowman, V. E., Woods, D. C., jan 2016. Emulation of multivariate simulators using thin-plate splines with application to atmospheric dispersion. SIAM/ASA Journal on Uncertainty Quantification 4 (1), 1323–1344.
URL https://doi.org/10.1137/140970148

[6] Burgin, L., Ekström, M., Dessai, S., jan 2017. Combining dispersion modelling with synoptic patterns to understand the wind-borne transport into the UK of the bluetongue disease vector. International Journal of Biometeorology 61 (7), 1233–1245.
URL https://doi.org/10.1007/s00484-016-1301-1

[7] Dabberdt, W. F., Miller, E., jan 2000. Uncertainty, ensembles and air quality dispersion modeling: applications and challenges. Atmospheric Environment 34 (27), 4667–4673.
URL https://doi.org/10.1016/s1352-2310(00)00141-2

[8] Duchenne, C., Armand, P., Marcilhac, M., Girard, S., Yalamas, T., 2017. A new method for assessing the uncertainty associated with 3d dispersion simulations in any variable meteorological conditions. In: 18th International Conference on Harmonisation within Atmospheric Dispersion Modelling for Regulatory Purposes, HARMO18. Bologna, Italy.

[9] Fukunaga, K., Olsen, D. R., feb 1971. An algorithm for finding intrinsic dimensionality of data. IEEE Transactions on Computers C-20 (2), 176–183.
URL `https://doi.org/10.1109/t-c.1971.223208`

[10] Galmarini, S., Bianconi, R., Klug, W., Mikkelsen, T., Addis, R., Andronopoulos, S., Astrup, P., Baklanov, A., Bartniki, J., Bartzis, J., Bellasio, R., Bompay, F., Buckley, R., Bouzom, M., Champion, H., D'Amours, R., Davakis, E., Eleveld, H., Geertsema, G., Glaab, H., Kollax, M., Ilvonen, M., Manning, A., Pechinger, U., Persson, C., Polreich, E., Potemski, S., Prodanova, M., Saltbones, J., Slaper, H., Sofiev, M., Syrakov, D., Sørensen, J., der Auwera, L., Valkama, I., Zelazny, R., sep 2004. Ensemble dispersion forecasting – part i: concept, approach and indicators. Atmospheric Environment 38 (28), 4607–4617.
URL `https://doi.org/10.1016/j.atmosenv.2004.05.030`

[11] Garaud, D., Mallet, V., oct 2011. Automatic calibration of an ensemble for uncertainty estimation and probabilistic forecast: Application to air quality. Journal of Geophysical Research 116 (D19).
URL `https://doi.org/10.1029/2011jd015780`

[12] Garaud, D., Mallet, V., 2012. Uncertainty estimation and decomposition based on monte carlo and multimodel photochemical simulations. Tech. Rep. 7903, Inria.
URL `https://hal.inria.fr/docs/00/67/83/06/PDF/RR-7903.pdf`

[13] Girard, S., Iovleff, S., 2008. Auto-associative models, nonlinear principal component analysis, manifolds and projection pursuit. In: Lecture Notes in Computational Science and Enginee. Springer Berlin Heidelberg, pp. 202–218.
URL `https://doi.org/10.1007/978-3-540-73750-6_8`

[14] Girard, S., Korsakissok, I., Mallet, V., 2014. Screening sensitivity analysis of a radionuclides atmospheric dispersion model applied to the

Fukushima disaster. Atmospheric Environment 95 (0), 490–500.
URL http://www.sciencedirect.com/science/article/pii/S1352231014005317

[15] Girard, S., Mallet, V., Korsakissok, I., Mathieu, A., 2016. Emulation and sobol' sensitivity analysis of an atmospheric dispersion model applied to the fukushima nuclear accident. Journal of Geophysical Research: Atmospheres.
URL http://dx.doi.org/10.1002/2015JD023993

[16] Hanna, S., Chang, J., jan 2012. Acceptance criteria for urban dispersion model evaluation. Meteorology and Atmospheric Physics 116 (3-4), 133–146.
URL https://doi.org/10.1007/s00703-011-0177-1

[17] Hanna, S. R., Paine, R., Heinold, D., Kintigh, E., Baker, D., 2007. Uncertainties in air toxics calculated by the dispersion models aermod and iscst3 in the houston ship channel area. Journal of Applied Meteorology and Climatology 46 (9), 1372–1382.

[18] Houle, M. E., 2015. Inlierness, outlierness, hubness and discriminability: an extreme-value-theoretic foundation. Technical Report NII-2015-002E.

[19] IMPEL, 2013. Extended release of mercaptan at a chemical plant. Tech. Rep. 43616, French Ministry for Sustainable Development.
URL https://www.aria.developpement-durable.gouv.fr/wp-content/files_mf/FD_43616_rouen_GB.pdf

[20] Ismert, M., Durif, M., 2014. Accident de Lubrizol du 21 janvier 2013 – couplage dispersion du nuage odorant/plaintes et appreciation des risques sanitaires associes. Tech. Rep. INERIS-DRC-13-137709-03375B, Ineris.

[21] Jolliffe, I. T., Cadima, J., mar 2016. Principal component analysis: a review and recent developments. Philosophical Transactions of the Royal Society A: Mathematical, Physical and Engineering Sciences 374 (2065), 20150202.
URL https://doi.org/10.1098/rsta.2015.0202

[22] Klampanos, I. A., Davvetas, A., Andronopoulos, S., Pappas, C., Ikonomopoulos, A., Karkaletsis, V., apr 2018. Autoencoder-driven weather clustering for source estimation during nuclear events. Environmental Modelling & Software 102, 84–93.
URL https://doi.org/10.1016/j.envsoft.2018.01.014

[23] Korsakissok, I., Mathieu, A., et al., 2018. Guidelines for ranking uncertainties in atmospheric dispersion. Tech. Rep. Ares(2018)1172146, European joint programme for the integration of radiation protection research.

[24] Le, N. B. T., Mallet, V., Korsakissok, I., Mathieu, A., Perillat, R., Didier, D., Apr. 2018. Metamodeling and optimization of probabilistic scores for long-range atmospheric dispersion applied to the fukushima nuclear disaster. In: EGU General Assembly Conference Abstracts. Vol. 20. p. 17209.

[25] Le, N. B. T., Mallet, V., Korsakissok, I., Mathieu, A., Périllat, R., 01 2019. Calibration of a surrogate dispersion model applied to the fukushima nuclear disaster. In: 3rd International Conference on Uncertainty Quantification in Computational Sciences and Engineering (UNCECOMP 2019). Greece, pp. 215–228.

[26] Mallet, V., Tilloy, A., Poulet, D., Girard, S., Brocheton, F., jul 2018. Meta-modeling of ADMS-urban by dimension reduction and emulation. Atmospheric Environment 184, 37–46.
URL https://doi.org/10.1016/j.atmosenv.2018.04.009

[27] Oldrini, O., Armand, P., jan 2019. Validation and sensitivity study of the PMSS modelling system for puff releases in the joint urban 2003 field experiment. Boundary-Layer Meteorology 171 (3), 513–535.
URL https://doi.org/10.1007/s10546-018-00424-1

[28] Oldrini, O., Armand, P., Duchenne, C., Olry, C., Moussafir, J., Tinarelli, G., Oct 2017. Description and preliminary validation of the pmss fast response parallel atmospheric flow and dispersion solver in complex built-up areas. Environmental Fluid Mechanics 17 (5), 997–1014.
URL https://doi.org/10.1007/s10652-017-9532-1

[29] Pearson, K., nov 1901. LIII. on lines and planes of closest fit to systems of points in space. The London, Edinburgh, and Dublin Philosophical Magazine and Journal of Science 2 (11), 559–572.
URL https://doi.org/10.1080/14786440109462720

[30] Roustant, O., Ginsbourger, D., Deville, Y., 2012. DiceKriging, DiceOptim: two R packages for the analysis of computer experiments by kriging-based metamodeling and optimization. Journal of Statistical Software 51 (1), 1–55.

[31] Skamarock, W. C., Klemp, J. B., Dudhia, J., Gill, D. O., Barker, D. M., Wang, W., Powers, J. G., 2005. A description of the advanced research wrf version 2. Tech. rep., National Center For Atmospheric Research Boulder Co Mesoscale and Microscale Meteorology Div.

[32] Swallow, B., Rigby, M., Rougier, J., Manning, A., Lunt, M., O'Doherty, S., 2017. Parametric uncertainty in complex environmental models: a cheap emulation approach for models with high-dimensional output. arXiv preprint arXiv:1702.03696.

[33] Tinarelli, G., Mortarini, L., Castelli, S. T., Carlino, G., Moussafir, J., Olry, C., Armand, P., Anfossi, D., mar 2013. Review and validation of MicroSpray, a lagrangian particle model of turbulent dispersion. In: Lagrangian Modeling of the Atmosphere. American Geophysical Union, pp. 311–328.
URL https://doi.org/10.1029/2012gm001242

[34] Trini Castelli, S., Armand, P., Tinarelli, G., Duchenne, C., Nibart, M., nov 2018. Validation of a lagrangian particle dispersion model with wind tunnel and field experiments in urban environment. Atmospheric Environment 193, 273–289.
URL https://doi.org/10.1016/j.atmosenv.2018.08.045

[35] Warner, T. T., Sheu, R.-S., Bowers, J. F., Sykes, R. I., Dodd, G. C., Henn, D. S., 2002. Ensemble simulations with coupled atmospheric dynamic and dispersion models: Illustrating uncertainties in dosage simulations. Journal of Applied Meteorology (1988-2005) 41 (5), 488–504.
URL http://www.jstor.org/stable/26184992

[36] Zhang, Y., Bocquet, M., Mallet, V., Seigneur, C., Baklanov, A., dec 2012. Real-time air quality forecasting, part II: State of the science, current research needs, and future prospects. Atmospheric Environment 60, 656–676.
URL https://doi.org/10.1016/j.atmosenv.2012.02.041